Numerical analysis of timber-to-timber joints and composite beams with inclined self-tapping screws

Chiara Bedon[a], Massimo Fragiacomo[b,c,*]

[a] University of Trieste, Department of Engineering and Architecture, Trieste, Italy
[b] University of L'Aquila, Department of Civil, Construction-Architectural and Environmental Engineering, L'Aquila, Italy
[c] National Research Council of Italy – Trees and Timber Institute (CNR IVALSA), San Michele all'Adige, Italy

A R T I C L E I N F O

Keywords:
Timber-to-timber joints
Composite beams
Inclined screws
Self-tapping screws (STSs)
Finite-Element (FE) numerical models
Cohesive Zone Modelling (CZM) method
Cohesive damage
Push-out tests
Full-scale bending experiments

A B S T R A C T

In this paper, a Finite-Element (FE) numerical investigation on timber-to-timber joints and composite beams with inclined self-tapping screws (STSs) is presented. Based on past experimental data and numerical literature efforts, full 3D solid FE models of selected geometrical and mechanical configurations of technical interest are implemented in ABAQUS software package and analysed under static loading conditions. The typical push-out samples include GL24h timber members with several types (WT-T-8.2, 190 mm and 220 mm their length), layouts (2 + 2, 4 + 4, 2 + 2 X-shaped) and inclination of screws (up to ± 45°). For the full-scale beam samples in bending (8 m their span), composite systems consisting of GL24h timber beam, wooden plank, spruce floorboards and STSs are investigated. There, the STS joints take the form of two-rows or X-shaped connections, respectively (45° or 90° their inclination), including four screw types and different spacing. In both the push-out and full-scale cases, simple modelling approaches are taken from the ABAQUS library and adapted to the timber-to-timber structural system under investigation, so as to explore their structural performance in the elastic and post-damage phases, up to failure. A key role in the typical FE models is assigned to input material properties and mechanical contacts, including damage constitutive laws so as to reproduce possible local failure phenomena in the timber or steel components, as well as cohesive damage interactions for the joints. The presented FE models are calibrated in accordance with past research studies, and validated – for the examined structural typology – against experimental results available in literature. Comparative calculations are hence presented, based on the collected numerical, experimental and analytical estimations for the selected samples. As shown, the examined modelling approach can reasonably capture the expected performance of timber-to-timber joints and composite systems.

1. Introduction and state-of-the-art

Self-tapping screws (STSs) are largely used in timber construction, both for fastening and as reinforcement. Their continuous thread with high withdrawal capacity makes it possible to construct many geometrical configurations for connections with increased stiffness and load-carrying capacity with respect to traditional timber-to-timber joints, particularly when the screws are used with an inclined configuration with respect to the timber grain. The arrangement of screws with different inclination and spacing, however, requires the designer to account for several aspects in the actual load transfer mechanism of the connection, including the bending capacity of screws, the embedment strength of wood, the withdrawal capacity of fasteners, as well as the friction between the system components. In this regard, the available analytical formulations for the prediction of the expected stiffness and load-carrying capacity of timber-to-timber screwed connections (see [1–5], etc.) are often only partially capable to capture the actual mechanical performance of inclined STSs configurations, hence resulting in approximate predictions only and requiring advanced theoretical models [6,7] or extended, dedicated experimental investigations. So far, several research studies have been focused on the experimental assessment of timber-composite connections, so as to overcome the actual gaps in design knowledge. Major literature studies include small and/or full-scale timber-to-timber specimens with inclined STSs (see for example [8–12]), but also several timber-concrete solutions ([13,14], etc.), while novel hybrid possibilities for timber-to-timber beams with inclined STSs have been explored in [15,16]. In [17], extended withdrawal experimental studies have been discussed for STS joints in Cross Laminated Timber systems, including variations in geometrical features and moisture conditions.

* Corresponding author at: Via Giovanni Gronchi 18 – Zona industriale di Pile, 67100 L'Aquila, Italy.
E-mail address: massimo.fragiacomo@univaq.it (M. Fragiacomo).

Accepted 14 September 2018

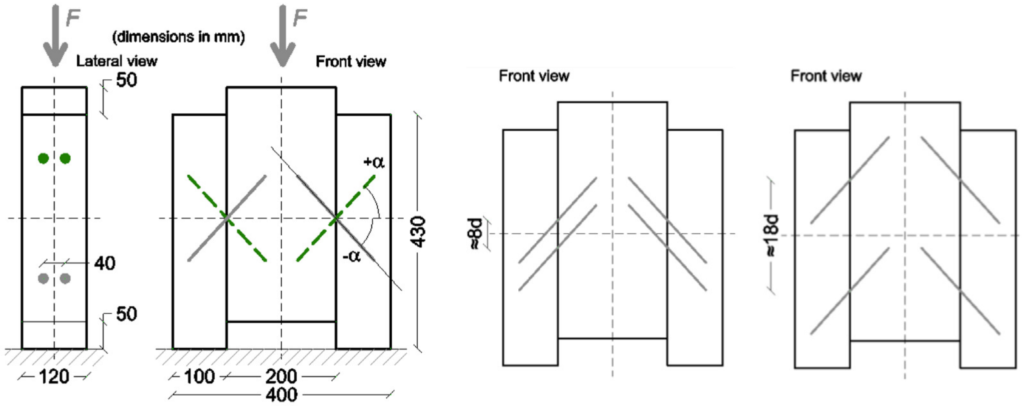

(a) S#1 and S#4 samples (b) S#2 samples (c) S#3 samples

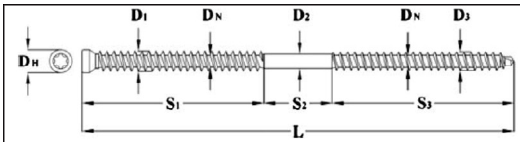

Key:

(a) screws for specimens with α= 0°, ±15° or (b) α= ±30°, ±45°

Type	L	S_1=S_3	S_2	D_1	D_2	D_3	D_N	D_H
D1-8.2×190 (a)	190	80	30	8.2	6.3	8.9	5.4	10
D1-8.2×220 (b)	200	95						

(d)

Fig. 1. Push-out experiments on timber-to-timber joints with inclined STSs, in accordance with [6]. (a) Elevation of the reference specimen, with typical geometrical properties, and (b)-(c) variations in the configuration of screws, with (d) corresponding nominal dimensions.

In this regard, Finite Element analyses (FE) can offer a robust support to design enhancements, as an alternative to costly and time consuming experimental testing [18–28]. A key aspect of such FE models is represented by the accurate description of the mechanical properties of the composite assemblies, including global stiffness and load-carrying capacity estimations, as well as the prediction of the reciprocal mechanical interaction between the system components. Full 3D continuum-based FE models can capture both local and global phenomena of the examined specimens, hence allowing a detailed insight into the actual mechanical response of timber-to-timber composite systems.

In this paper, the major outcomes of a numerical investigation carried out in ABAQUS [29,30] on timber-to-timber push-out specimens and composite beams loaded in bending are reported. The numerical estimations are validated towards experimental test results [6,8], including various geometrical and mechanical configurations of inclined STSs.

A key aspect in the full 3D solid models herein discussed is represented, as also in accordance with [31], by the implementation of a fictitious ‘soft layer’ with cohesive damage interactions, at the interface between the steel STSs and the surrounding timber components. Compared to other modelling approaches, the Cohesive Zone Modelling (CZM) method has well-known intrinsic advantages, since it does not need: (i) pre-existing definition of cracks, (ii) prior assumptions for onset and growth of damage, (iii) complex moving mesh techniques, and (iv) a very dense mesh definition close to the cracks (to ensure local occurrence of infinite stress and strain peaks). Major structural applications available in the literature are related to several typologies of composite systems and joints (see [32–37], etc.). The available research applications, on the other hand, are limited in number and type, for timber structural systems. These include refined attempts to account for delamination and inter-fiber cracks in LVL or CLT assemblies (see for example [38–40]). Small-scale samples (timber-to-concrete, notched composite joints with steel screws) have been investigated in [41], where a single cohesive layer was used to account for shear cracking of timber, close to the notch. Janssens [42] used cohesive elements in the advanced FE modelling of dowelled connections in LVL systems, with careful consideration for embedment tests. Four separate layers of cohesive elements were used, in the locations of the expected cracks for timber. The adopted implicit solver generally gave evidence of the FE model complexity and sensitivity to a set of parameters, but also resulted in hard convergence achievement for the simulations.

In [43], a preliminary extension of the CZM modelling approach proposed in [31] has been considered for timber-to-timber push-out joints with inclined STSs. There, the CZM technique was used in combination with the fictitious ‘soft layer’, at the interface between the screws and the timber members. The ABAQUS/Explicit solver was chosen [29,30], to stabilise the solution even in the damaged phases. This paper hence follows and extends the preliminary observations of [43], aiming at giving evidence of the FE-to-experimental comparative results and possible critical issues/limits of the numerical method, for the specific structural typology of timber-to-timber composite systems with inclined STSs. Selected numerical results are discussed for some configurations of technical interest, including both push-out samples (Section 4) and full-scale composite beams (Section 5).

2. Reference experimental tests

The numerical study herein discussed is based on the past push-out and bending experimental results carried out on timber-to-timber joints and composite beams with inclined STSs, as reported in [6,8]. Key features of specimens and methods are summarised in Sections 2.1 and 2.2.

2.1. Small-scale push-out specimens

Following the [44,45] provisions, a wide set of push-put experiments (64 specimens in total) was investigated in [6], to assess the stiffness properties and load-carrying capacity of inclined screws, by varying the inclination α, the number and position of fasteners, the loading direction (shear-tension and shear-compression experiments). In accordance with Fig. 1, the typical specimen consisted of three spruce, glued laminated timber beams, with GL24h their strength class according to EN 1194 [46].

Double-thread, carbon steel STSs (L = 190 mm and 220 mm their nominal length), WT-T-8.2 type from Rothoblaas [47,48] were used to realise the mechanical connection. The full experimental investigation included four specimen types, see Fig. 1(a)-to-(c) for a schematic layout. There, the S#1-to-S#4 labels are used to identify push-out specimens characterised by:

- S#1 = 2 + 2 screws (with α = 0°, ± 15°, ± 30°, ± 45° the tested configurations)
- S#2 = 4 + 4 screws, a_1 = 70 mm ≈ 8d their distance (α = 0°, ± 15°, ± 30°, ± 45°), where $d = D_3$
- S#3 = 4 + 4 screws, a_1 = 160 mm ≈ 18d their distance (α = 0°, ± 15°, ± 30°, ± 45°)
- S#4 = 2 + 2, X-shaped screws (α = 0°, 15°, 30°, 45°)

The test measurements (load-displacement curves) were hence post-processed so as to derive the typical ultimate resistance and stiffness of the examined samples. In doing so, most of the experimental specimens gave evidence of a “type f” ductile rupture mode, consisting in wood embedment and in the occurrence of two plastic hinges in the screws, as also in accordance with the corresponding analytical predictions. Despite such a rather close correlation between test results and analytical estimations – including the stiffness and resistance calculations – the experimental programme also highlighted the need of additional extended testing on timber-to-timber composite joints with inclined STSs, so as to collect and assess a consistent number of samples (i.e. repetitions for each series, and joint features). In this context, the first potential of the FE models herein discussed lies in the possibility of further extending the available experimental studies reported in [6], hence allowing the user to account for variations in geometrical and mechanical features in similar joints (i.e. number and properties of STSs, resistance class of timber, etc.), as far as the working assumptions and input features are properly validated. At the same time, an intrinsic advantage of the same FE models is the possibility of monitoring the progressive damage evolution in each sample component, for several loading ratios and up to failure, with respect to experimental samples that can hardly allow for a detailed, visible step-by-step analysis of damage evolution (see also [41]).

2.2. Full-scale bending specimens

The full-scale experimental tests reported in [8] were then taken into account, as a benchmark to validate the FE models. The typical specimen consisted of a 150 × 200 mm^2 GL24h glulam beam (8000 mm the nominal span and 7500 mm the distance between its end hinge supports), with a 500 × 80 mm^2 thick, GL24h board on the top. A non-structural layer of 180 × 30 mm^2 floorboards (spruce) was also interposed between the beam and the plank, see Fig. 2, so as to fill the 30 mm thick gap. Four different configurations of timber-to-timber joints with inclined STSs (herein labelled as B#1-to-B#4 type samples) were considered in the original experimental programme, including variations in the screw type (SFS WT-T-8.2, VGZ9320, HBS10200 types from type from Rothoblaas [47,48]), length (300 mm, 320 mm and 200 mm respectively), nominal diameter, thread (double, full or single), arrangement of STSs (double row or X-shaped) and inclination (α = 45°, 90°), see Fig. 3 and [8]. A variable spacing s (100 mm or 200 mm) was also considered for the screws, so as to optimise the connections along the beams span.

According to the test setup schematised in Fig. 2, vertical loads were applied on the reference, simply supported specimen, so as to reproduce the effect of a uniformly distributed load. During the past tests, a set of Linear Variable Displacement Transducers (LVDTs) was used to monitor the vertical displacement of the B#1-to-B#4 samples under the imposed loads, including relative slip measurements at the beams ends. Preliminary elastic bending tests were also carried out before the destructive experiments (three repetitions for each plank and timber beam), so as to estimate the actual longitudinal Modulus of Elasticity (MOE) for the timber components. Further preliminary testing included elastic bending experiments on the B#n samples, when deprived of mechanical fasteners, aiming at assessing the flexural performance of the assembled planks and beams in the so called *layered* configuration (i.e. weak shear connection).

Such a series of test measurements generally highlighted a certain scatter in the MOE values for the planks and beams, compared to nominal product properties (see Section 3). Differing from the push-out samples recalled in Section 2,2, the destructive bending tests suggested a rather comparable bending performance for the B#n samples under ordinary loads, even in presence of different STSs arrangements, hence suggesting a minimal influence of the joint features for service design conditions. The limited number of test samples and measurements reported in [8], however, can offer only partial feedback and would suggest the extension of the full-scale investigations.

2.3. Background

Timber-to-timber composite beams attracted, like timber-to-concrete assemblies, the attention of a wide number of research studies, due to their large use in novel or existing buildings, and to the multitude of detailing and features for the available technological solutions (i.e., type and features of fasteners, etc.). For design purposes, both serviceability and ultimate limit states performances must be ensured for them, under short and long-term loading conditions. Analytical models of practical use hence represent, since the 40’s, an attractive alternative to more onerous calculation methods and/or full-scale testing, and are mostly derived from the governing differential equations of composite beams with partial composite behaviour (see [49,50], etc.). Within the available closed-form solutions, the simplified γ-method adopted by the Eurocode 5 (Part 1-1, Annex B) is conventionally used for linear elastic calculations, and proved to offer rather good estimations for timber composite beams with closely spaced fasteners [51–53]. According to Fig. 4, the Newmark’s original formulation has been also successfully applied and/or adapted to other structural typologies, including mechanical fasteners or continuous adhesive joints (see for example [53–58], etc.) typically assumed to have a linear elastic response and uniform stiffness along the span. In [8], for example, the analytical estimation of the bending response for the B#n samples of Fig. 3 was carried out by accounting for the actual spacing of fasteners (see Section 5), and the basic governing equations for the equilibrium of a given timber-to-timber composite system were set to (X^i, with i = I,…IV is the i-th derivative of each X quantity):

$$N_1^{II} - \frac{k_c^I}{k_c} - k_c N_1 \left[\frac{EI_\infty}{EA_0 EI_0} \right] = k_c \frac{M}{EI_0} a \qquad (1)$$

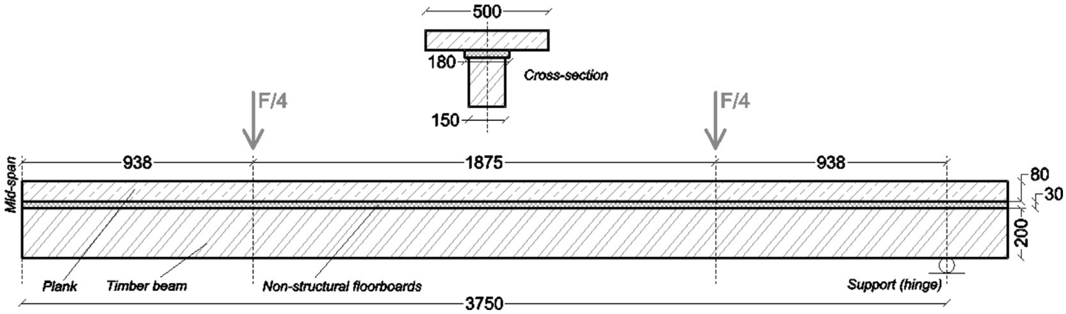

Fig. 2. Bending tests on timber-to-timber composite beams. Test setup according to [8] – All the nominal dimensions are given in mm.

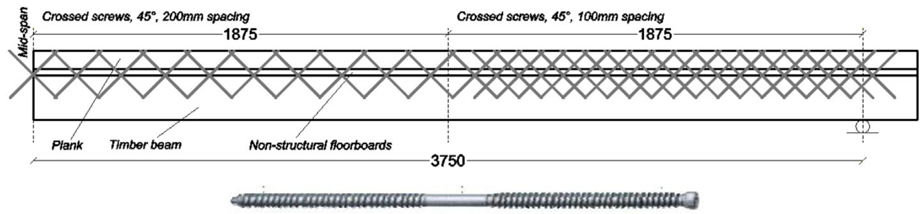

(a) B#1 (SFS WT-T-8.2 screws)

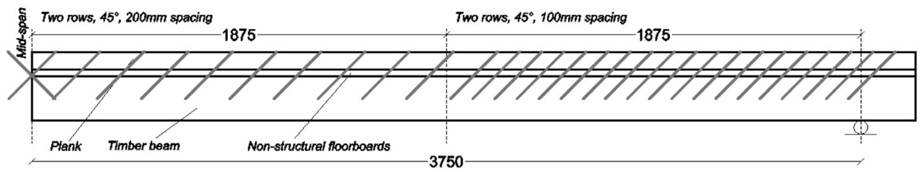

(b) B#2 (SFS WT-T-8.2 screws)

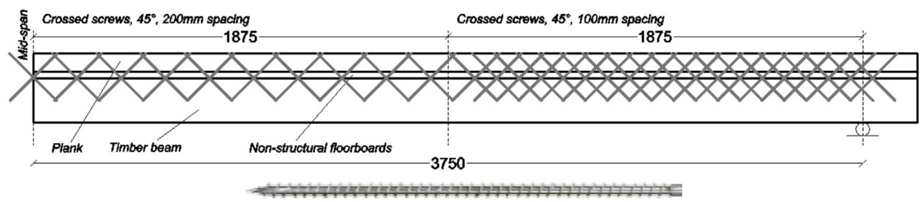

(c) B#3 (VGZ9320 screws)

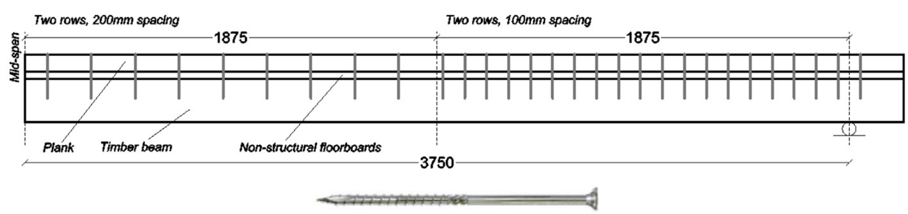

(d) B#4 (HBS10200 screws)

Fig. 3. Bending tests on timber-to-timber composite beams, with different joint configurations, according to [8].

$$w^{IV} - \frac{k_c^I}{k_c} w^{III} - k_c \left[\frac{EI_\infty}{EA_0 EI_0} \right] w^{II} = -\frac{1}{EI_0} M^{II} + \frac{1}{EI_0} \frac{k_c^I}{k_c} M^I + k_c \left[\frac{EI_\infty}{EA_0 EI_0} \right] M \tag{2}$$

There, N_1 represents the axial force in the component (1), while w is the expected beam deflection. Denoted by a the distance between the centerline of the upper (1) and lower (2) beam components, with M the applied bending moment, the deflection w is related to the ideally rigid flexural stiffness EI_∞ of the composite system ($k_c \to \infty$, *monolithic limit – full*), to the flexural stiffness EI_0 of the beam without any shear connection ($k_c \to 0$, *layered limit – abs*), and to the corresponding axial stiffness EA_0.

The distributed stiffness of the connection, k_c, includes major uncertainties for the related analytical calculations, even under short-term loading, being largely affected by several geometrical parameters [6,7]. Its reference value – especially in the case of timber-to-timber or timber-concrete composites structures with metal fasteners – is usually smeared along the beam span, via an equivalent spacing s_{eq}. This is not the case of the study reported in [8], where k_c was indeed calculated via a Fourier transform, so to allow for more accurate predictions.

Despite past efforts aimed at providing enhanced analytical formulations for design, most of the simplified analytical formulations lack of consideration for several aspects (i.e. plasticity, time-dependent phenomena for the beam components, local damage, etc.) that in the case of timber composite systems may have severe effects on the overall

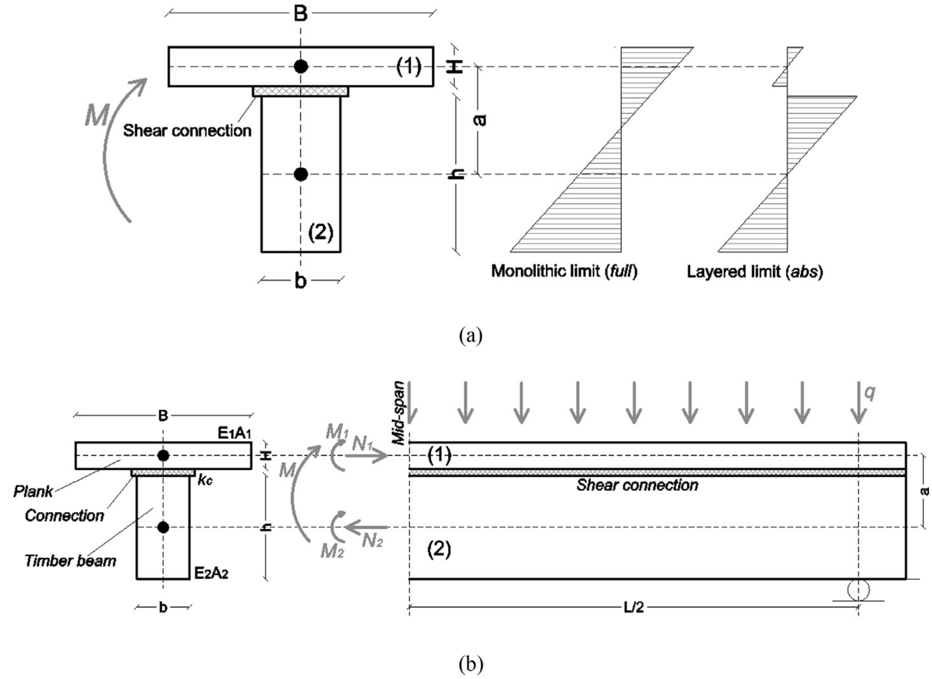

Fig. 4. Composite beams in bending. (a) Typical stress-strain distribution, depending on the efficiency of the shear connection and (b) mathematical model.

structural performance. The maximum resistance of screwed joints is also difficult to analytically predict [6], hence requiring experimental testing, both at the small and full-scales.

In this context, FE numerical models – even based on simplified assumptions but accurate and reliable in the description of material and components behaviours – can offer a further insight on the full response of the timber-to-timber systems herein investigated, and of composite structural assemblies in general. The use of equivalent springs representative of the load-slip response of fasteners (i.e. from small-scale experiments), for example, is a conventional, suitable and computationally efficient approach in timber engineering (see for example [59–63], etc.). Such an assumption is particularly reliable when the fastener load-bearing response in each principal direction is mostly independent. For the specific case of inclined STSs for timber-to-timber composite beams, however, stiffness and resistance parameters can be sensitive to the joint arrangement [6–8] as well as to the combination of axial and shear/lateral loads (see for example [64,65]), or possible local effects that push-out testing does not capture, hence suggesting – at least for a preliminary insight – the use of more accurate modelling techniques.

3. Finite element numerical study

Throughout the full parametric numerical investigation, similar FE assumptions and methods were used to schematise both the small-scale and the full-scale composite specimens of Sections 2.1 and 2.2.

3.1. General modelling assumptions and solving method

The numerical simulations were carried out using the ABAQUS/Explicit software package [29], in the form of quasi-static imposed displacement histories for the examined composite systems. The Explicit solver was specifically chosen to facilitate the convergence of simulations, when accounting for the damage initiation and progressive evolution in the assembly components (i.e. material side) as well as at their interfaces (i.e. cohesive damage interactions and surface contacts), see Section 3.2. The goal was in fact to properly describe the actual test loading condition for the push-out and beam samples subject of investigation, including estimations for the elastic and post-damaged phases, up to failure, via commercially available input options. In this regard, the chosen solving method enhance the potential of FE models to predict the overall structural performance of timber-to-timber joints and composite beams. In this study, the 'deletion' of failed timber or steel mesh elements was disregarded, to ensure a stable convergence of the simulations, due to the presence of several contact interactions for the involved damaging components. The quasi-static deformation of the specimens was then controlled – throughout the parametric Explicit simulations – by monitoring the estimated energy balance [30].

Given the similar modelling approach for the small-scale and full-scale assemblies, major variations between them were represented by trivial geometrical detailing (and hence mesh features) and boundary/loading conditions, so as to account for the test setup configurations of Figs. 1(a) and 2.

For all the push-out models, the FE assemblies were subjected to an imposed linearly increasing, vertical displacement, being assigned to the top face of their central timber member. For each simulation, the relative slip of these timber components, as well as the corresponding base reaction force, were hence continuously monitored over the full step time, so as to collect the corresponding force-slip characteristic curves. Accordingly, the bending test setup of composite specimens in Figs. 1 and 2 was carefully reproduced in the performed quasi-static, numerical analyses. In this latter case, load-control simulations were carried out, and the total load vs. mid-span deflection of each beam specimen was monitored, for comparative purposes with test measurements.

3.2. Push-out specimens

3.2.1. Model assembly, mechanical interactions and cohesive contacts

The typical model consisted, for all the specimen components, of 8-node 3D solid elements, C3D8R-type stress-strain bricks with reduced integration, as available in the ABAQUS library [30].

The computational cost of Explicit simulations – being sensitive to mesh refinement and solver assumptions – was minimized by taking advantage of specimens features schematised in Fig. 1, hence 1/4th of the nominal geometry for the S#1, S#2 and S#3-type joints and 1/2th of the nominal geometry for the S#4-type joints (with appropriate mechanical boundary conditions along symmetry planes), were

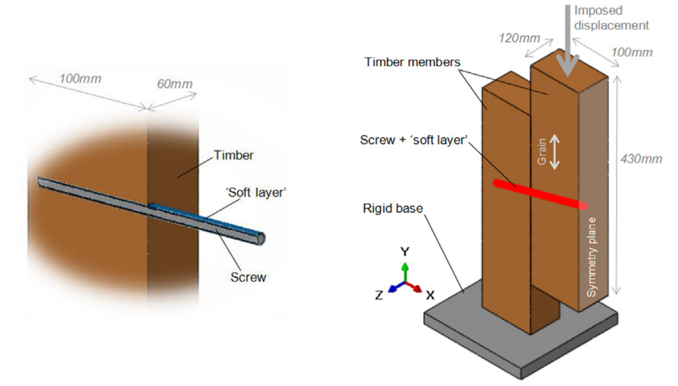

(a) (b)

Fig. 5. FE modelling of push-out timber-to-timber joints with inclined STSs (example for the S#1-type specimens). 3D view of (a) typical joint detail (cross-section; in evidence, the 'soft layer' surrounding each STS) and (b) corresponding FE assembly – 1/4th the sample geometry (ABAQUS, with hidden mesh pattern).

considered, respectively.

A rigid base support was also described via C3D8R-type, 3D solid elements, so as to schematically reproduce the testing machine and the related effects (i.e. compared to idealised nodal restraints for the timber elements) on the actual deformation of the specimens (see Fig. 5(b)).

Based on [31], major simplifications in the joints detailing were then focused on the geometrical description of steel STSs and their mechanical interaction with the surrounding timber parts (see Fig. 5(a)). In particular, see also [31,47], each screw was reproduced in the form of an equivalent, circular cross-section with uniform diameter equal to the outer thread size of screws, i.e. D2 = 6.3 mm (see Fig. 1(d)) and *L* the nominal length. A 'soft layer', being representative of STSs threads and timber fibres was then interposed at the interface between each screw and the surrounding timber members, with 8.2 mm the outer diameter (i.e. D1 in Fig. 1(d)). As also discussed in [31], such a fictitious soft layer and the related cohesive interaction – given the typically high withdrawal strength of STSs – aims at accounting for possible brittle failure mechanisms at the screw-to-timber interface, specifically for possible damage occurring for shear or tension perpendicular to the grain. The assumed material properties (see also Table 1 and Section 3.2.2) were hence derived in [31,66] with the support of tests, so as to reproduce a complex medium in which steel and timber (C24 the resistance class) could interact (i.e. threads region). The method presented in [31,66] follows preliminary studies, see [67], where time-consuming and weakly convergent FE assemblies inclusive of the STS threads were first proposed. The approach was also in line with [68], where small-scale joints with a single STS perpendicular to the grain and under axial loads were investigated. Also in that case, the STS threads were numerically reproduced, to capture local stress distributions in the wooden member, but timber properties (i.e. radial MOE and compressive strength) were numerically fitted, so as to match the load-displacement test data.

In this study, the optimisation of mesh size and pattern represented the first issue of the full FE investigation, requiring preliminary sensitivity studies. Due to variations in the geometrical features of the S#1-to-S#4 type samples and modifications in the STSs inclination, separate sensitivity analyses and specific meshing rules were required for each set of push-out FE models. For the sake of clarity, such preliminary investigations are not included in the paper, but generally resulted in the use of a swept (advancing font) meshing technique, with an average element size minimised in the region of the STSs (0.3 mm-to-0.5 mm the reference dimension for the screws, the 'soft layer' and the timber elements in the region of the holes). The maximum element size (i.e. for the steel rigid base and the lateral portions of timber elements), at the same time, was in the order of 5-to-8 mm. The so defined meshing approach resulted in S#*n* push-out FE assemblies typically characterised by a variable number of solid elements and DOFs, up to average values of 80,000 and 240,000 respectively for 1/4th the nominal geometries (and up to an average amount of 140,000 elements and 400,000 DOFs, for some of the S#4 samples).

A key role was finally assigned to mechanical contacts and interactions for the so described FE components, so as to reproduce the actual behavior of the timber and steel parts within the push-out samples under investigation. Given the reference FE assembly agreeing with Fig. 5, tangential 'penalty' and normal 'hard' *surface-to-surface* behaviors were first defined for the timber-to-timber surfaces in contact, to account for the relative slip and for the potential separation of the timber components, during the overall loading phase. There, the static friction coefficient was set equal to μ = 0.5, in accordance with [69]. A similar *surface-to-surface* contact interaction (with μ = 0.2 the corresponding friction coefficient [69]) was then assigned to the interface between the base face of the specimen (i.e. external timber member) and the rigid steel support representative of the testing machine (see Fig. 5(b)). In this way, the occurrence of local deformations during the push-out loading stage was properly taken into account. Compared to ideal boundary restraints (see also [41]), the use of contact interactions for the base support of FE samples proved in fact to have a crucial role on their actual performance, especially in terms of local stresses.

Each steel screw and the surrounding 'soft layer' were then rigidly connected via a '*tie*' mechanical constraint, hence enabling relative rotations and displacements among the interested nodes. The external surface of the 'soft layer' and the adjacent timber elements were indeed interrelated via a '*cohesive contact*' interaction. There, special care was spent to model both the elastic stiffness and the damage input data. For the radial, longitudinal and normal stiffnesses (i.e., being representative of the interface stiffnesses prior to damage onset), the '*default contact enforcement method*' was used. In terms of damage at the 'soft layer'-to-timber interface, being expected to initiate together with the failure propagation in timber (see also the resistance values reported in Table 1), the maximum nominal stress (MAXS) criterion was used. Accordingly, the *'damage initiation criterion'* was detected as a combination of stresses so that:

$$\max\left\{\frac{t_n}{t_n^0}, \frac{t_s}{t_s^0}, \frac{t_t}{t_t^0}\right\} = 1, \tag{3}$$

where the variables t_n^0, t_s^0 and t_t^0 represent the maximum allowable values of nominal stresses when the deformation is purely normal (*n*) to the bonding interface or in the first (*s*) or second (*t*) shear directions. Within the available damage criteria in ABAUQS, the Eq. (3) represents one of the available options only. According to the quadratic nominal stress criterion (QUADS), for example, the failure initiation condition is given by:

Table 1
Input properties for the equivalent 'soft layer' and for the corresponding cohesive damage interaction (ABAQUS), in accordance with [31,46,66].

'Soft layer' moduli (mean values, in MPa)	Longitudinal (i.e., cylinder axis) and tangential	370
	Shear	720
	Radial	50
'Soft layer' failure	Max. shear (MPa)	5
	Damage evolution/ displacement (mm)	Linear/4
Cohesive damage contact resistance (mean values, in MPa)	Longitudinal	37.55
	Transverse	3.85
	Shear	3.85
	Rolling shear	3.5

$$\left\{\frac{t_n}{t_n^0}\right\}^2 + \left\{\frac{t_s}{t_s^0}\right\}^2 + \left\{\frac{t_t}{t_t^0}\right\}^2 = 1. \tag{4}$$

Even both the MAXS and QUADS criteria of Eqs. (3) and (4) are stress-based, the first approach disregards any possible relationship between the different stress directions, while the QUADS criterion assumes a quadratic relationship among the stresses recorded in the principal directions. For the analysis of timber components, the MAXS approach was hence herein preferred.

The same MAXS approach was also preferred to other separation damage criteria from the ABAQUS library (i.e., MAXU and QUADU [30]), due to major uncertainties on the calibration input data. For the MAXU and QUADU options, the failure initiation conditions are in fact in close correlation with Eqs. (3) and (4), but input data are represented by allowable contact separation values (instead of allowable stresses), that would be hardly estimated for timber members. Following [31] and Eq. (3), the reference stress values for damage initiation were in fact defined in this study by accounting for the mean timber mechanical properties, as separately detected for the normal, tangential and radial directions. Finally, a linear *damage evolution* law was set for the degradation of mechanical contact properties, with full residual stiffness for the cohesive contact interactions at the first attainment of 4 mm deformation [31]. The so defined cohesive damage interaction was combined with a tangential penalty/normal hard behaviour, as previously described. In this manner, once attained the failure condition for the cohesive contact region, a reliable performance of the FE samples was ensured, avoiding the compenetration of screws in the adjacent timber components.

3.2.2. Materials

Both timber and steel constitutive laws were described – where available – by taking into account the experimental mechanical properties provided in [6,8], as well as product standards and appropriate damage models, to include possible failure mechanisms in all the specimen components.

As reported in [6], at the time of push-out experiments, carbon steel screws (10.9 the nominal resistance class) were in fact tested in uniaxial tension, with $f_{u,m} = 940.3$ MPa and $f_{u,k} = 934.3$ MPa ($f_{u,k} = 1000$ MPa the nominal value) the obtained mean and characteristic ultimate stress values. The resulting isotropic, elasto-plastic Von Mises constitutive law of carbon steel was hence defined by accounting for $E = 210$GPa and $\nu = 0.3$ as nominal MOE and Poisson' ratio, with $f_y = f_u = 940.3$ MPa the yielding/ultimate stress values. An ultimate strain $\varepsilon_u = 0.5\%$ was also considered.

Spruce is an orthotropic material at both the macro and microscale [70] – therefore it was defined as an orthotropic media with brittle elastic behaviour. As also in accordance with [31], given the grain direction and loading condition of Fig. 5(b), the Hill plastic criterion was used to specify appropriate resistance values along the principal directions of interest for the timber components. Assuming $E_\perp = 390$ MPa and $E_{||} = 11.6$GPa as the nominal mean MOE values for the directions perpendicular and parallel to the grain respectively, $G = 690$ MPa was taken into account for the longitudinal shear modulus [46,71]. The radial MOE of timber was set equal to $E_\perp$. For the Hill plastic law, nominal mean resistance values were also considered, based on the specifications of product standards for GL24h strength class timber (see [46,71]), so as to reproduce in a simplified way a reliable performance for the assembled push-out FE models. While allowing anisotropic plastic laws, the Hill formulation has the intrinsic limit of assuming symmetry for compression and tension in each principal direction, hence requiring special attention for timber. Accordingly, see Fig. 5(b), the compressive resistance parallel to the grain (i.e. Y local axis) was set to $f_{c,0} = 37.5$ MPa. In this paper, the remaining Hill stress ratios were then calculated along the other directions (i.e. X, Z, and XY, XZ, YZ planes for the shear components) so as to reproduce the mean compressive resistance perpendicular to the grain ($f_{90,c} = 3.57$ MPa, X and Z axis) and the mean shear strength $f_v = 3.85$ MPa (XY, XZ, YZ). Such a simplified assumption is also in line with [41], where push-out timber-concrete composite samples were numerically investigated by allowing for relevant material strengths only, hence adapting ordinary ABAQUS library material laws (in place of advanced user subroutines, etc.) for the loading and boundary conditions of interest.

A brittle failure criterion was also defined for the timber members, so as to reproduce possible local failure phenomena, especially in the region of joints. Once attained the ultimate resistance (and in particular, the compressive strength perpendicular to the grain $f_{c,90}$, for the timber elements in contact with the screws), a linear damage propagation was assumed. In this study, due to lack of more appropriate input data and testing feedback, the degradation of timber mechanical properties was set to coincide with a full damage evolution, at the first attainment of 4 mm of deformation (see [31]). In this specific context, the input features were reasonably adapted from [31], given the similarity in the resistance class for the wooden elements (GL24h and C24 respectively). The extension of the FE modelling technique to other STS samples, including different materials, should be hence carefully assessed and validated.

In the case of the equivalent 'soft layer', finally, being characterised by an indefinitely linear behaviour, the elastic mechanical properties of GL24h timber were again considered. The only variation was represented by the radial MOE, where a fictitious value of of 50 MPa was taken into account (see Table 1 and [31,66]). In this way, based also on the cohesive interaction input of Table 1, possible local numerical effects leading to unreliable/inconsistent stress values were in fact prevented through the parametric investigation. At a preliminary stage, FE sensitivity studies highlighted that such a MOE can be roughly set equal to the rolling shear modulus of wood. Higher input values, conversely, would negatively impact on the overall FE estimations, since alterating the bending stiffness of STSs. In this regard, it is important to point out that the given input features should be properly calibrated, when considering different structural systems and/or wooden resistance class, compared to the selected samples. The general robustness and reliability of the FE modelling technique herein discussed, in other words, should be properly assessed and supported by testing.

3.3. Full-scale beam specimens

The same FE modeling approach summarised in Section 3.2 for the push-out samples was successively used and adapted to the full-scale timber-to-timber composite beams described in Section 2.2. Depending on the configuration of screws, see Figs. 2 and 3, a 1/4th or 1/2th of the nominal geometry of these specimens was considered for each test, see Fig. 6.

Within the full set of full-scale FE assemblies, even in presence of trivial variations in the geometrical features of STS joints, the reference model consisted of:

(i) the timber beam,
(ii) the wooden plank,
(iii) the steel STSs (each one of them inclusive of the 'soft layer' and accounting for the cohesive damage interaction technique described in Section 3.2), and
(iv) the non-structural layer of spruce floorboards, interposed between the timber beam and the plank.

A key role – in addition to the cohesive damage technique – was assigned to further *surface-to-surface* contacts, being representative of the mechanical interaction between the timber beam, the floorboards and the top plank. In the case of the non-structural floorboards, due to lack of mechanical fasteners, contact interactions were accounted on the top and bottom faces, as well as in the region of holes, so as to allow the possible separation from the other specimen components (when subjected to tensile deformations), as well as to transfer compressive

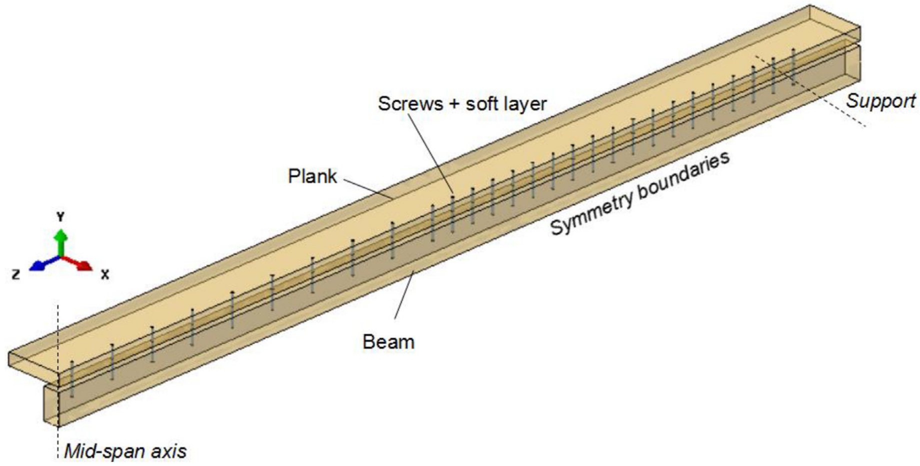

Fig. 6. FE modelling of timber-to-timber composite beams with STS connections (3D view from ABAQUS, with hidden mesh pattern). This example refers to the B#4 beam specimen (HBS10200 screws).

stresses between them.

In terms of material properties, special care was spent for the GL24h timber components. Given the availability of experimental testing on materials, the nominal longitudinal MOE of 11600 MPa conventionally assumed for the beam and plank [46] was in fact replaced by the corresponding mean MOE values experimentally derived in [8]. For the other moduli and resistance values, otherwise, mean nominal values were indeed taken into account, from product standards [46], as well as in accordance with Section 3.2. The so assembled composite beams were hence subjected to the loading and boundary configurations schematised in Fig. 2, with appropriate symmetry restraints.

4. FE push-out results and comparisons

Derivation of comparative experimental and FE results was carried out on the basis of FE numerical force-slip curves, for each one of the B#*n* examined configurations, and corresponding test data discussed in [6]. The maximum resistance $F_{\max}$ was numerically detected as the first condition occurring between the attainment of the (a) actual maximum load or (b) a load corresponding to a joint slip of 15 mm. Accordingly, the serviceability stiffness value K_{ser} was calculated in accordance with standard provisions [44].

In doing so, careful consideration was given to the damage initiation and propagation in each FE model component, so as to ensure the reliability of the extrapolated $F_{\max}$ and K_{ser} data. Based on the assigned surface-to-surface contacts (Section 3.2.1) and materials constitutive laws/interaction damage models (Section 3.2.2), the numerical failure of push-out specimens was typically observed to occur due to a combination of degradation phenomena, namely associated to (a) crushing in timber (i.e. in the region of screws); (b) yielding of screws and (c) severe damage at the screw-to-timber interface (cohesive damage), see Fig. 7. There, such an outcome is emphasised via selected contour plots for the S#1-type sample ($\alpha = 15°$), at an imposed slip of 12 mm. Worth of interest is that the non-dimensional 'CSMAXCRT' damage parameter of Fig. 7(d) – ranging from 0 to 1 for the undamaged and fully damaged configurations respectively – denotes a fully collapsed cohesive contact for ≈1/3rd the STS nominal length, with two visible plastic hinges in the screw (Fig. 7(c)). A rather limited crushed region can be perceived for the wooden region (i.e. red portions of Fig. 7(b)), which typically extended along the STS and coincided for the cohesive damaged region (see Fig. 7(d)). In the direction of the grain, see Fig. 7(b), the wooden fibres were then generally subjected to limited stresses, when progressively moving far away from the fasteners.

In general, the typical push-out analysis was then stopped due to convergence issues, in the very late damaged stage, for all the examined

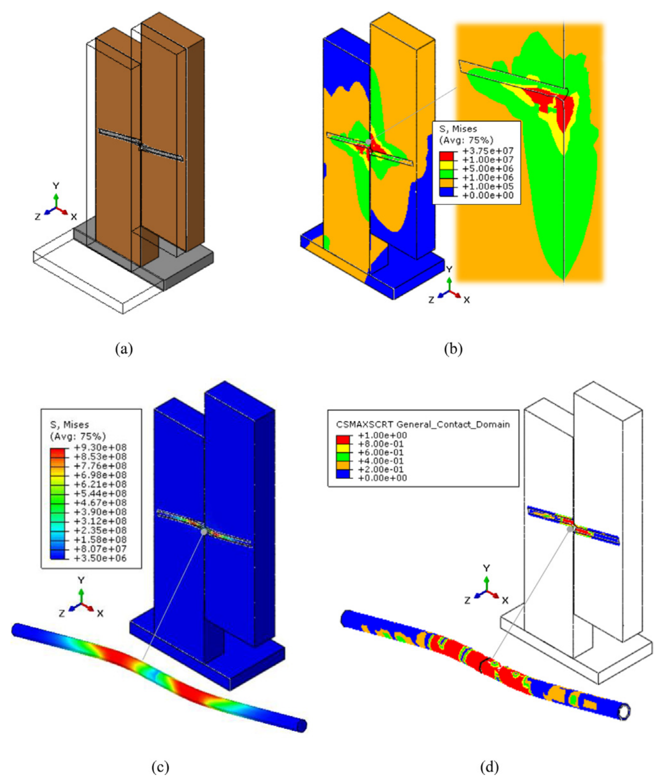

Fig. 7. Damage propagation in the push-out composite joints (ABAQUS, 3D cross-section). Example for the S#1-type specimens ($\alpha = 15°$). (a) Deformed configuration, with (b) timber local damage (stress values in Pa), (c) yielding of screws (stress values in Pa) and (d) cohesive damage (ABAQUS).

FE models. Such a numerical weakness, was observed to occur for slip ratios larger than the reference 15 mm, or in any case in the decreasing stage for the collected load-slip curves, hence did not affect the F_{max} and K_{ser} estimations briefly discussed in Sections 4.1, 4.2, 4.3.

4.1. *Maximum load F_{max}*

Globally, a rather good agreement was observed between the numerical and experimental maximum load values, for all the specimens series as well as by changing the inclination α of screws, within the same group of connections.

In Fig. 8(a), some comparisons are proposed in terms of maximum

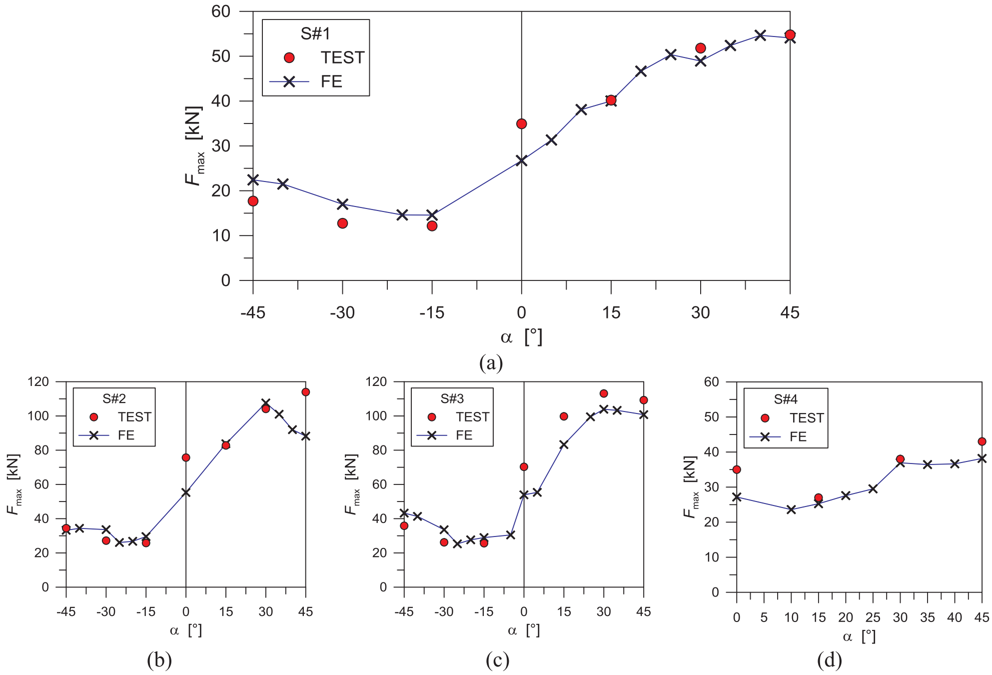

Fig. 8. Comparison between experimentally [6] and numerically (ABAQUS) predicted maximum loads (mean values), for the (a) S#1-type specimens, (b) S#2, (c) S#3 and (d) S#4.

resistance values for the S#1-type connections (i.e. with single fastener for each resisting section). As a general outcome of the overall parametric numerical simulations, see also Fig. 8(b)-to-(d), the FE models generally gave evidence of a mostly stable variation of the numerically estimated F_{max} values with α. Despite such a stable numerical dependency of F_{max} estimations on α, however, in some cases the scatter between numerical and past experimental predictions was found to be relevant.

In Table 2, comparative results are reported for the S#1-to-S#4 series of composite joints, giving evidence of the percentage scatter Δ between the mean experimental and numerical F_{max} results.

As shown, the numerical results were found to either underestimate or overestimate the corresponding experiments. As a general trend, in addition, the numerical estimations proved to be non-conservative for the experimental specimens in shear-tensile loads. In any case, maximum scatter values lower than ± 30% were obtained for all the examined configurations. In particular, such a kind of deviation of the FE estimations from the test daa was mainly observed for the joint specimens with fasteners perpendicular to the grain (α = 0°, for all the S#n series) or fasteners under shear-tensile loads with high inclination angles (α > 30°, for the S#2 series). A possible motivation could lie in localised numerical issues (i.e. singularities, materials features, or test setup boundaries). Given the lack of detailed experimental characterisation for the material properties of the joints components, as well as the limited number of test samples for each different configuration, the FE modelling approach herein discussed proved to offer reasonable estimations for the expected maximum load of timber-to-timber joints with inclined STSs. Additional extended investigation are in any case required, to properly assess the reliability of the same FE technique.

Table 2
Maximum load F_{max} for the S#1-to-S#4 push-out specimens: percentage scatter between experimental [6] and FE numerical (ABAQUS) predictions. $\Delta = 100 \times (X_{FE} - X_{TEST})/X_{TEST}$.

		Δ (%) Push-out series			
Loading protocol	α (°)	S#1	S#2	S#3	S#4
Shear-compression	−45	26.7	−3.5	20.6	/
	−30	33.7	23.5	28.2	/
	−15	19.9	14.6	12.9	−22.4
	0	−23.7	−26.8	−22.3	−6.4
Shear-tension	15	−0.5	1.2	−16.5	−2.8
	30	−5.6	3.4	−8.2	−11.2
	45	−1.3	−22.6	−7.7	−11.1
	Average	7.1	−1.5	1.0	± 9.2
	Standard deviation	± 20.4	± 18.3	± 19.5	/

4.2. Effective number of screws n_{ef}

Additional comparative results are given in Fig. 9 in terms of effective number of screws n_{ef}, being conventionally calculated as the ratio between the total resistance F_{max} of specimens with multiple aligned screws or single screws, respectively. Such a kind of comparison was performed by relating the S#2 and S#3 results to those of the S#1-type specimens, by varying the inclination α. Given the experimental and numerical data displayed in Fig. 8 and Table 2, the corresponding n_{ef} value was namely calculated as:

$$n_{ef}^{TEST\,\text{-}\,S_i} = n_{ef}^{FE\,\text{-}\,S_i} = \frac{F_{max}^{S_i}}{F_{max}^{S_1}}, \quad i = 2, 3 \tag{5}$$

The so derived values were also compared with the analytical estimations provided by the Eurocode 5 [5] for bolted connections, where the theoretical n_{ef} value is conventionally defined as:

$$n_{ef}^{EC} = \min\left(n;\, n^{0.9}\cdot\sqrt[4]{\frac{a_1}{13d}}\right) \tag{6}$$

In this research study, as also in accordance with [6], the value $d = 8.9$ mm was used in Eq. (6), with $n = 2$. The screws distance a_1 was hence set equal to 70 mm or 160 mm for S#2 and S#3 specimens respectively.

Comparative n_{ef} data are displayed in Fig. 9 for the S#2 and S#3-type joints. There, numerical results are proposed for the set of experimentally assessed α values, as well as for further intermediate α configurations numerically investigated, so as to explore more in detail

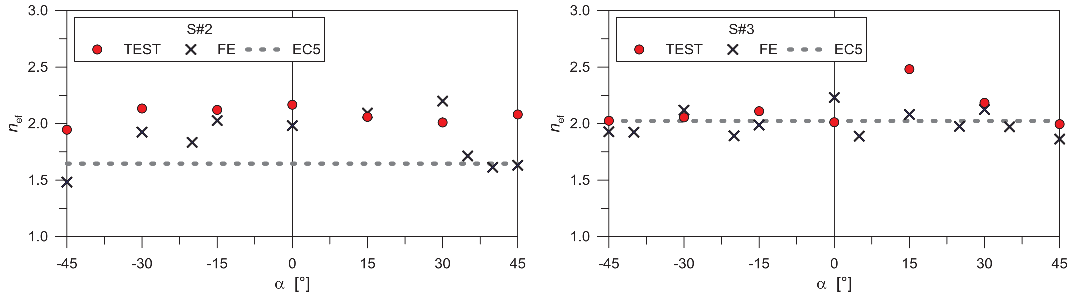

(a) (b)

Fig. 9. Comparison between experimentally [6], analytically (Eq. (6)) and numerically (ABAQUS) predicted values of effective screws (mean values), for specimen types (a) S#2 and (b) S#3.

the sensitivity of FE predictions to the STSs inclination. The collected FE data, see Fig. 9, gave evidence of a certain sensitivity of numerical predictions to possible local damage phenomena in the vicinity of the fasteners. Such an effect was especially perceived for the S#2-type connections, where the n_{ef} values numerically calculated were found to be mostly stable with α, with the exception of high α values (see for example the -45° and $+40^{\circ}$, $+45^{\circ}$ dots in Fig. 9(a)).

4.3. Elastic stiffness K_{ser}

At the final stage of the push-out comparative calculations, the elastic stiffness K_{ser} was also estimated for the examined STS samples. In Fig. 10, the mean experimental and FE numerical stiffness values are reported for the S#1-type specimens.

In general, a rather close correlation was observed for most of the S#1, S#2 and S#3 geometrical configurations, whose experimental and numerical average stiffness values are compared in Fig. 11. There, analytical calculations derived from the single or double stiffness methods presented in [6] are also collected. The gray region, finally, gives evidence of the standard deviation of the mean experimental results from [6]. Major scatter between numerical and experimental results was observed especially for high inclination values, both for shear-tension and shear-compression loading conditions (see for example $\alpha = \pm 45^{\circ}$, where the FE estimations both underestimate/overestimate the corresponding test results). The FE models also proved to underestimate the actual experimental measurements for shear-tensile loads. Such a scatter could be justified by experimental setup details – being numerically accounted in the form of mostly ideal loading and boundary configurations – as well as by possible uncertainties in the material mechanical properties, hence resulting in possible premature local damage.

For the X-shaped joints, see Fig. 11(b), major scatter was indeed observed, with up to 30–40% the difference with respect to the test data. The X-shaped connections, in this regard, proved to be more

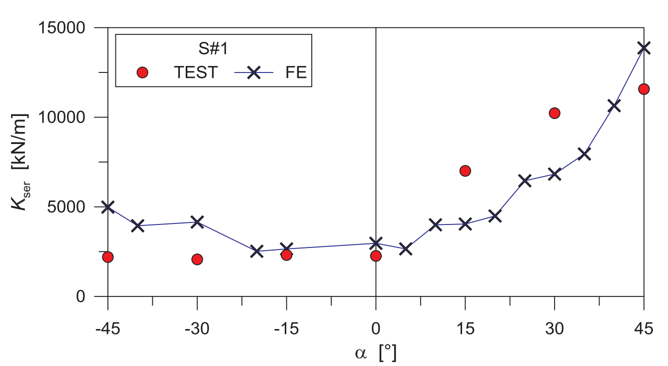

Fig. 10. Elastic stiffness K_{ser} for the S#1-type timber-to-timber joints, as obtained from past experiments [6] and FE numerical modeling (ABAQUS).

(a)

(b)

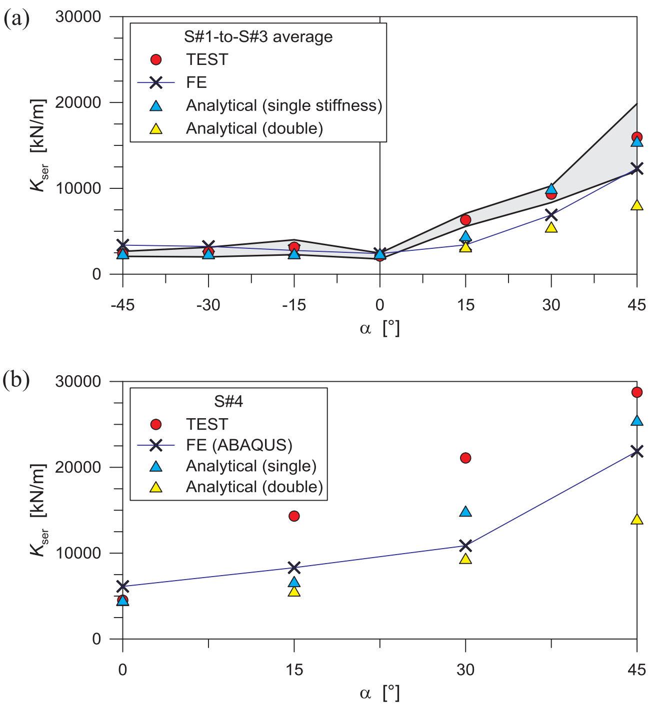

Fig. 11. Comparison among experimental [6], analytical [6] and numerical (ABAQUS) average stiffness values, (a) S#1-to-S#3 and (b) S#4-type joints.

sensitive to stiffness estimations, compared to the other S#1-to-S#3 samples, while rather good results were collected in terms of maximum resistance F_{max} for the same series of joints (see Table 2). Like in the case of shear-tensile S#1-to-S#3 average values, see Fig. 11(b), the FE models underestimates the actual experimental results, but the numerical predictions were found in any case to be comprised between the single/double stiffness analytical predictions derived from [6].

5. Discussion of FE full-scale bending results

The load-displacement responses of the full-scale bending specimens of Section 2.2 were then reproduced using the corresponding FE models, so as to explore the actual potential and limits of the examined modelling technique. For the sake of brevity, the B#3 sample is not included in this paper, due to strong similarity with the B#1 specimen.

In general, see also Section 2, the past experimental program demonstrated a nearly constant initial stiffness for all the full-scale specimens, even in presence of a clearly different number and inclination of screws, see Fig. 12(a). The exception was represented by the B#4 specimen (X-shaped joints), where a marked decrease in the beam stiffness was recorded. In any case, a rather similar collapse mechanism

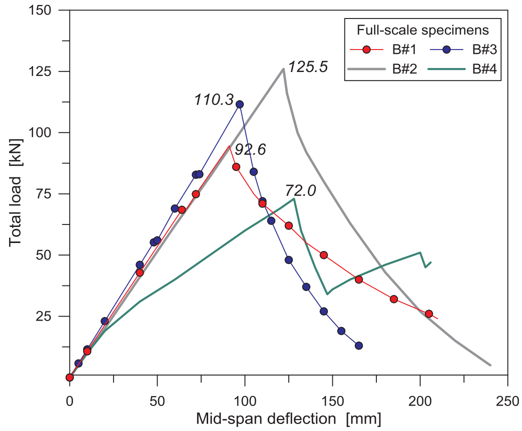

(a)

(b)

Fig. 12. Past full-scaletests on the B#1-to-B#4 composite beams, in accordance with [8]. (a) Experimental load-deflection response and (b) typical failure mechanism in the timber beams.

was observed for all the full-scale samples, with a tensile/bending failure mechanisms of the timber beam in close correlation with Fig. 12(b).

Through the FE investigation, the modelling approach herein discussed was assessed towards the past experimental observations, including comparisons of load-deflection curves for all the samples, as well as a qualitative comparison of the expected collapse configuration for them. Further efforts for the reliability assessment of FE results were derived from analytical calculations reported in [8] for the same beam samples. The so collected comparative results are summarised in the following section. The B#3 sample, being characterised by strong similarity in the geometrical and mechanical features with the B#1 specimen, is not explicitly discussed in the paper, but proved to be in close correlation with the other FE assemblies and samples, see Sections 5.1, 5.2, 5.3, 5.4.

5.1. Preliminary calculations under service loads

At a preliminary stage of the comparative study, some first estimations are proposed for the B#*n* samples, so as to assess the FE accuracy in the elastic stage, with respect to the full-scale experiments and selected analytical models from the literature. In doing so, the B#*n* specimens were assumed to be loaded with service design loads (4 kN/m^2 the magnitude, corresponding to 15 kN in total for the test setup of Fig. 2). In Table 3, the so calculated mid-span deflections are proposed, as obtained respectively from (i) the past experiments [8], (ii) the analytical model described in Section 2.3 (values taken from [8]), (iii) the γ-method in use in the Euroocode 5 (values taken from [8]) and (iv) the FE assemblies herein presented. The corresponding connection efficiency η_w is also reported for the same samples, giving evidence – as also discussed in [8] – of mostly rigid STS joints.

Table 3
Mid-span deflection for the B#n beam specimens under service design loads (4kN/m^2, or 15kN for the test setup of Fig. 2), as obtained experimentally [8], analytically [8] and numerically (ABAQUS). $\Delta = 100 \times (X_i - X_{TEST})/X_{TEST}$.

	Mid-span deflection [mm]			
	B#1	B#2	B#3	B#4
Test [8]	13.29	14.74	12.82	12.56
Analytical [8]	12.34	14.10	11.94	16.47
Analytical – Eurocode 5 [8]	12.16	13.85	11.76	16.77
FE (ABAQUS)	12.20	15.35	12.01	15.35
	Δ [%]			
Analytical [8]	−7.1	−4.3	−6.9	31.1
Analytical – Eurocode 5 [8]	−8.5	−6.0	−8.3	33.5
FE (ABAQUS)	−8.2	4.1	−6.3	22.2
	η_w [%]			
Analytical [8]	94.6	96.3	95.1	95.5

Compared to the past test results, it is possible to perceive from Table 3 that both the analytical and numerical models generally tend to underestimate the expected deflection for the examined samples (with an average scatter of −8%, for the B#1, B#2 and B#3 samples), hence resulting in overall non-conservative predictions. This is not the case of the B#2 numerical assembly (4.1% the scatter, which is in contrast with the unsafe analytical estimations). For the B#4 specimen, finally, the analytical and numerical models resulted in overestimated deflections, up to ≈34% larger than the experimental sample, but with improved estimations for the FE assembly (22% the scatter).

Given such a generally good correlation between FE models and data from literature, the numerical investigation was hence further extended for the selected B#*n* samples in bending, up to collapse. Major comparative results are summarised and discussed in the following sections.

5.2. B#2beam specimen

The FE analysis of the B#2 specimen with SFS WT-T-8.2 × 300 screws ($\alpha = 45°$) was stopped at the attainment of the maximum load-carrying capacity of the experimental specimen, as obtained by accounting for damage initiation and propagation in the beam components. Globally, the FE model proved to offer a very good correlation with the experimental load-displacement curve, see Fig. 13(a). Fig. 13(b) and (c), accordingly, present the cross-sectional and 3D views of the B#2 beam specimen at a maximum displacement of 150 mm, with evidence of Von Mises stresses (values are given in Pa) for the FE assembly components.

As expected, the beam failure configuration was typically characterised by cracking on the timber, rather than severe damage in the STSs. This is in line with test observations [6,8], where higher sensitivity of push-out series of samples was generally observed, by changing the joint features. For the ultimate configuration of the FE model corresponding to the experimental collapse, in particular, maximum stresses in the steel screws were found in the order of 240 MPa, hence suggesting a premature failure mechanism in the specimen due to tensile damage propagation in the timber beam.

A mostly linear response was in fact predicted for the FE model, even though a slight decrease of the assembly stiffness can be perceived as far as the total applied load exceeds 100kN. In this context, the elastic stiffness of the B#2 test sample was correctly captured by the FE

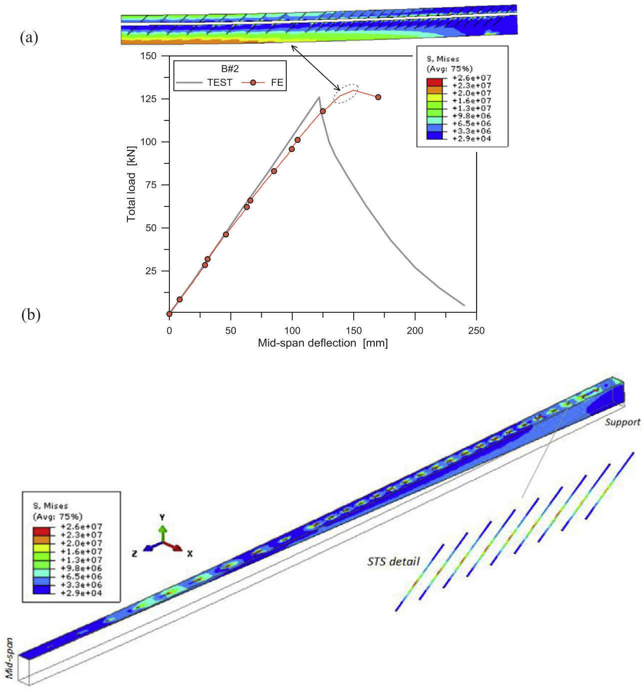

Fig. 13. B#2 beam specimen. (a) Experimental and numerical load-deflection response, with (b) Von Mises contour plots at 150 mm of displacement (longitudinal cross-section and 3D view, with evidence of the timber beam and selected STSs) – Stress values are given in Pa.

model, due to accurate estimation of the mechanical performance of each single components as well as their reciprocal interaction. Such a numerical decrease in the elastic stiffness for loads higher than ≈90–100 kN proved to derive – in the post-processing stage – from damage propagation in the timber components, and especially in the timber beam in bending, due to the attainment of maximum tensile stresses close to mid-span, in the order of 26 MPa (see in Fig. 13(b) the stress contour plot for the timber components).

Compressive stress peaks were also observed around the steel fasteners (Fig. 13(b)), but crushing phenomena resulted mostly negligible, with respect to tensile and cohesive damage mechanisms.

The CZM technique, in particular, typically resulted in early damage propagation for the interface elements of all the joint components, with maximum stresses exceeding the assigned limit values (i.e. Table 1) from the initial loading phase (see Fig. 14). There, the red regions give evidence of full damage for most of the screws, even at only 20 mm of vertical deflection of the beam.

Table 4
Mechanical performance parameters for the B#2 beam specimen, as obtained experimentally [8], analytically [8] and numerically (ABAQUS). $\Delta = 100 \times (X_{FE} - X_{TEST})/X_{TEST}$. Key for damage = T: tensile rupture of timber beam; C: crushing of timber beam; Y: screws yielding; CH: cohesive.

	Beam elastic stiffness [kN/mm]	Ultimate load [kN]	Beam stress/ Tension side [MPa]	Collapse mechanism
Experiment [8]	1.07	125.5	38.5	T
Analytical – Eurocode 5 [8]	1.06	78.2	24.0	T
FE (ABAQUS)	0.99	128.6	27.0	T + CH
Δ [%]	−7.3	2.4		

Table 4 summarises a further comparison for the mechanical response of the B#2 beam. The experimental results are reported, including Eurocode 5 analytical predictions (values derived from [8]) and FE estimations, so as to give evidence of the rather good accuracy of numerical results (with stiffness and ultimate load numerical predictions in the range of −7% and +3% the test results). It can be clearly noticed that the analytical calculations offer a rather close correlation with the experiment as far as the elastic stiffness is taken into account (−1% the test estimation), while the failure configuration for the B#2 sample is strongly underestimated (−38% the experimental collapse). The governing collapse mechanism is also reported in Table 4, for the same B#2 sample. From a numerical point of view – given the early cohesive damage propagation (i.e. Fig. 14) and the assigned mechanical properties – such a failure configuration was defined based on post-processing analysis of stress scenarios in the assembly components.

5.3. B#4 beam specimen

In Fig. 15, the experimental and numerical responses of the B#4 specimen (see Fig. 3) are shown. Compared to the B#2 specimen, variations included the type ((i.e., two rows of HBS10200 fasteners, in place of WT-T screws) and inclination of fasteners (α = 90°, rather than 45°, with 100 mm and 200 mm their spacing).

The experimental sample failed at an imposed load of 72 kN, corresponding to a mid-span deflection of ≈130 mm. While the FE models emphasised a certain reliability of numerical estimations for the examined specimens, major scatter and uncertainties were observed for the B#4 specimen, being characterised by a specific experimental behaviour (see also the load-deflection comparative plots of Fig. 12(a)).

The numerical simulations gave evidence of a fairly good correlation with the experimental stiffness of the B#4 specimen, for the first loading stage. A mostly linear response was however numerically

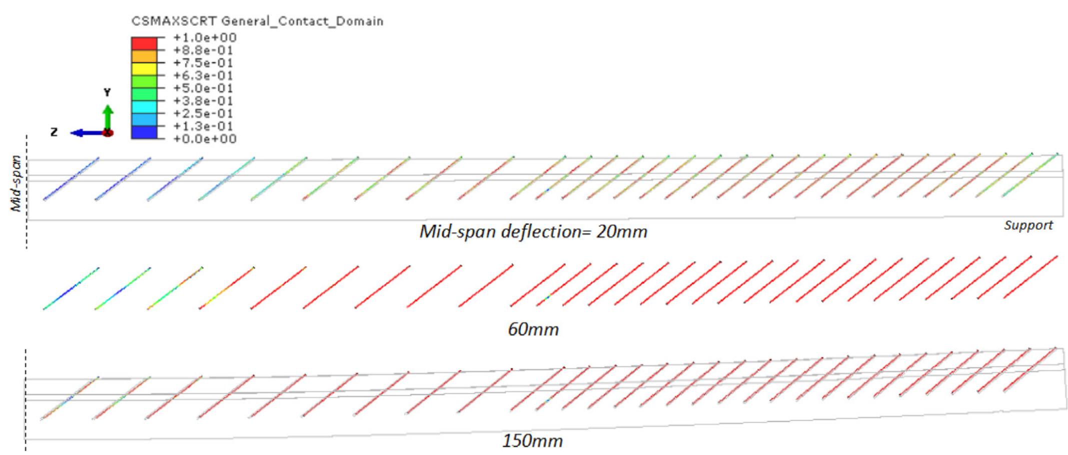

Fig. 14. B#2 beam specimen. Cohesive damage propagation in the joints, as a function of the beam mid-span deflection (ABAQUS).

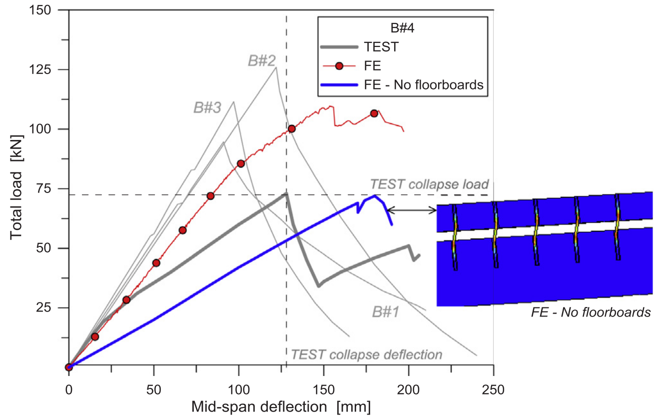

Fig. 15. B#4 beam specimen, experimental and numerical load-deflection response (in evidence, the ultimate configuration for the STSs close to the beam supports (ABAQUS)).

predicted, in accordance with the other experimental samples, see Fig. 15 ('FE' curve). As a result – while both the damage evolution in the beam components and failure mechanism were estimated by the FE model in close correlation with the B#2 (and other) specimen – the same FE model typically proved to overestimate the ultimate stiffness and resistance for the sample under investigation.

For a mid-pan deflection of 130 mm corresponding to the experimental collapse, see Fig. 16, maximum tensile stresses in the timber beam were again found to lie in the order of ≈25 MPa, hence denoting the incipient tensile/bending failure mechanisms that was experimentally observed (i.e., Fig. 12(b)).

Crushing phenomena were also noticed in the wooden components, in the vicinity of the joints, due to exceedance of the compressive resistance parallel to the grain for timber (see the box selection in Fig. 16). Maximum stresses in the STSs were indeed found in the range of ≈380 MPa, with local stress peaks up to ≈730 MPa for the screws at 1/3rd the beam span (see the detail view in the contour plot of Fig. 16), hence denoting a mostly elastic behaviour of fasteners.

In order to further assess the possible reasons for such an abrupt variation in the stiffness of the B#4 experimental sample, the same beam specimen was hence numerically investigated by fully neglecting the intermediate floorboards layer, being typically responsible of additional bending and axial stiffness for the composite system, as well as of a certain local restraint for the bending deformation of screws. Such a numerical configuration can be regarded as a lower limit condition for the B#4 sample.

As shown in Fig. 15, see the 'FE – No floorboards' plot, a mostly linear elastic response was again predicted for the B#4 numerical assembly, even with evidence of a marked decrease in terms of elastic stiffness, compared to the nominal B#4 specimen, from the early loading stage. Premature yielding of some STSs was however predicted, starting from a mid-span deflection in the order of 80 mm and further propagating in all the screws (see the detailed contour plot of Fig. 15). Compared to the nominal geometrical configuration for the B#4 sample, limited peak stresses were predicted in the timber beam, with ≈18–20 MPa for the tensile side of the beam and a lack of evident crushing mechanisms in the vicinity of the STS joints. The ultimate resistance of the numerical B#4 beam system, equal to ≈73 kN and in close correlation with the experimental observations, was fully governed by damage in the STS connections.

In this context, the FE feedback suggests that the past experimental results could have been partly affected by local damage mechanisms in the floorboards-to-joints connections, hence justifying the variation in the load-displacement slope, with respect to the other full-scale samples. The availability of a single repetition for each experimental specimen, however, is strictly related to intrinsic uncertainties. Table 5, finally, summarises some major mechanical observations for the B#4 beam sample. The collected values remark, as shown, how the FE model can closely match the experimental stiffness and ultimate resistance, as far as the floor board is considered or not. The analytical calculations according to the Eurocode 5 can offer reliable estimations for the elastic stiffness of the B#4 sample (−4.4% the test result), but tend to underestimate the ultimate failure condition (−13% the test collapse load).

5.4. B#1 beam specimen

Finally, the B#1 beam specimen characterised by X-shaped joints was numerically investigated. In Fig. 17, the experimental and numerical load-displacement curves are shown, including – for joint similarity – the B#3 experimental values.

As shown, the FE model proved again to properly capture the elastic stiffness of the composite assembly. Worth of interest is the close correlation with test predictions, while the X-shaped push-out joints were found to have major scatter in the estimation of the elastic stiffness of small-scale joints (see Section 4). Such a finding suggests the high potential of the modelling technique herein assessed, but also the high

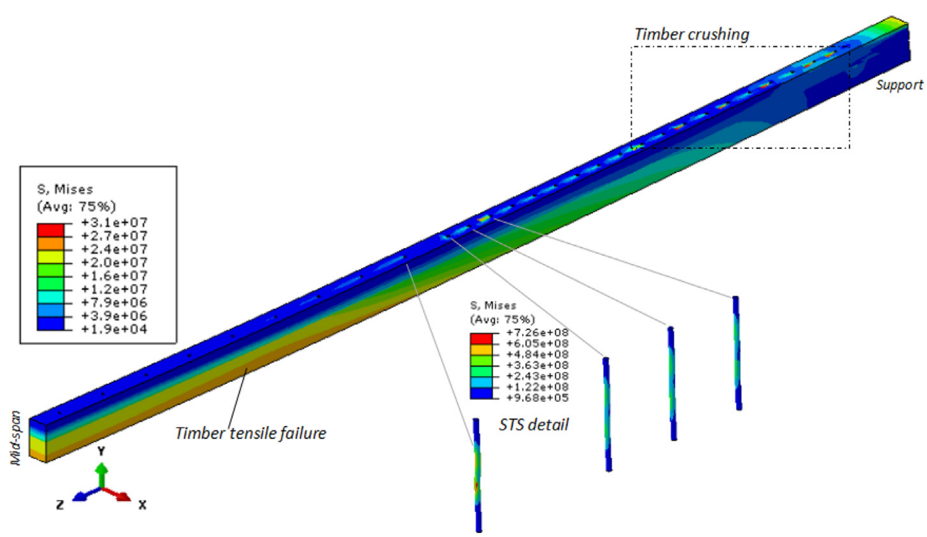

Fig. 16. B#4 beam specimen. Maximum stresses in timber, as observed at 130 mm of mid-span vertical displacement, with evidence of the STS response – Stress values are given in Pa (ABAQUS, 3D view of the timber beam and selected STSs).

Table 5
Mechanical performance parameters for the B#4 beam specimen, as obtained experimentally [8], analytically [8] and numerically (ABAQUS). $\Delta = 100 \times (X_{FE} - X_{TEST})/X_{TEST}$. Key for damage = T: tension timber beam; C: crushing timber beam; Y: screws yielding; CH: cohesive.

	Beam elastic stiffness [kN/mm]	Ultimate load [kN]	Beam stress/ Tension side [MPa]	Collapse mechanism
Experiment [8]	0.95	72.0	27.6	T
Analytical – Eurocode 5 [8]	0.91	62.6	24.0	T
FE (ABAQUS)	0.85	103.3	25.0	T + C + CH
Δ [%]	−9.5	43.0		
FE – No floorboards (ABAQUS)	0.41	72.9	20.0	Y + CH
Δ [%]	−57.1	1.2		

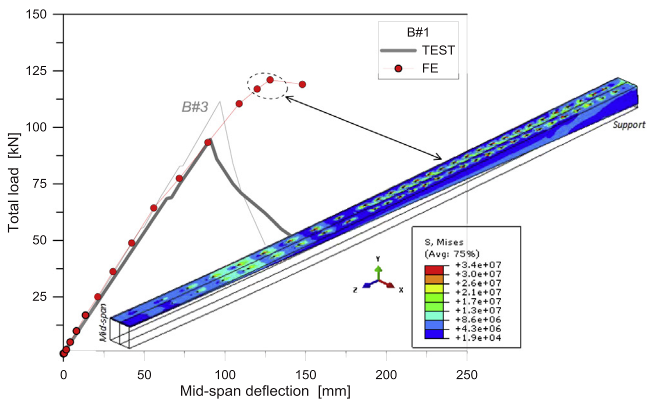

Fig. 17. B#1 beam specimen. (a) Experimental and numerical load-deflection response, with evidence of stress distribution in the timber beam (values are given in Pa), at a maximum deflection of 130 mm (ABAQUS).

sensitivity of results to the test setup and loading protocol (i.e. push-out versus full-scale bending experiments), as well as the mostly different mechanical response of STS joints in each of the examined testing configurations.

The FE model for the B#1 beam assembly typically resulted in a linear elastic response. A slight decrease in the beam stiffness can be perceived only for total loads higher than 70-80kN. This variation was found to be related to damage propagation in the timber components, especially crushing mechanisms close to the steel fasteners, as also numerically observed for the other full-scale assemblies, see the stress contour plot provided in Fig. 17. The damage propagation in the timber and steel components was found to numerically agree with the B#2 and B#4 beam samples earlier discussed. In Table 6, major output data are

Table 6
Mechanical performance parameters for the B#1 specimen, as obtained experimentally [8], analytically [8] and numerically (ABAQUS). $\Delta = 100 \times (X_{FE} - X_{TEST})/X_{TEST}$. Key for damage = T: tension timber beam; C: crushing timber beam; Y: screws yielding; CH: cohesive.

	Beam elastic stiffness [kN/mm]	Ultimate load [kN]	Beam stress/ Tension side [MPa]	Collapse mechanism
Experiment [8]	1.03	92.6	29.9	T
Analytical – Eurocode 5 [8]	1.22	74.3	24.0	T
FE (ABAQUS)	1.19	121.3	26.0	T + C + CH
Δ [%]	15.4	30.9		

proposed for the examined FE system. Compared to the B#2 and B#4 beam specimens, as shown, the FE model generally overestimates the actual bending stiffness and ultimate resistance of the full-scale sample, up to ≈16% and 30% respectively the test results. The analytical calculations according to the Eurocode 5 provide indeed an elastic stiffness that is apparently in line with the FE model (+19% the test results). The expected failure load for the B#1 sample is however analytically predicted in ≈75kN, that is -20% the experimentally observed collapse.

6. Conclusions

In this paper, the structural performance of timber-to-timber joints and composite beams with inclined self-tapping screws (STSs) was numerically investigated. The FE modelling assumptions were validated towards past experimental results of literature, being representative of timber-to-timber specimens with different arrangement and features for the STSs joints. Comparative results were hence critically discussed in the paper, both for push-out and full-scale beam specimens, including analytical calculations derived from existing models, design standards and experimental observations from past literature projects.

Through the FE parametric investigation, as shown, a key role was assigned to timber material properties but especially cohesive interface damage contacts and fictitious ‘soft layers’, being properly calibrated so as to take into account for possible localeffects in the region of joints. As shown, the proposed FE approach generally gave evidence of fairly close correlation with the reference experimental test results, both for the push-out specimens and the full-scale samples.

For the small-scale push-out specimens, in particular, an average scatter of −25% or +10% was generally observed, for the load-bearing estimations in shear-compression and shear-tension, respectively. Major deviations of FE models from the testswere mainly observed for small-scale specimens characterised by the presence of screws with high inclination α for the fasteners (± 40° or ± 45°, in the current study), hence suggesting possible numerical issues due to mostly local effects, as well as possible uncertainties on the material properties and on the idealised description of the test setup. In any case, given the fairly limited number of experimental test repetitions for each geometrical configuration, acceptable estimations were generally achieved from the FE simulations.

A good match with the experimental results was also observed for the mechanical response of full-scale composite beams in bending, especially in terms of elastic stiffness for the examined samples, hence denoting the high sensitivity of the actual mechanical response of inclined STS connections to the loading configuration. The FE models offered also a close correlation with the experiments in terms of ultimate configuration at collapse, highlighting in detail the propagation of damage mechanisms and the effects of possible non-structural details (i.e. the floorboards layer). In this sense, the FE technique herein discussed suggested a certain potential for the numerical analysis and design optimisation of timber-to-timber composite joints and beams with inclined STSs. Before the FE approach could be recognised as robust tool in place of time and cost consuming experiments, however, further extended investigations are however required to properly assess the presented FE modelling technique, including additional variations in the geometrical and mechanical properties for samples of technical interest.

Acknowledgments

DPC-ReLUIS – Year 2017 is gratefully acknowledged for partially funding the research activity within the framework of the ‘PR4-Timber structures’ Italian project.

The Italian Ministry of the University is also gratefully acknowledged for partially funding the research presented in this paper as a part of the Research Projects of National Interest PRIN 2015 Prot. 2015YW8JWA “The short supply chain in the biomass-timber sector:

procurement, traceability, certification and Carbon Dioxide sequestration".

References

[1] Johansen KW. Theory of timber connections. International association of bridge and structural engineering. Bern 1949;9:249–62.
[2] Blaß HJ, Bejtka I, Uibel Y. Tragfähigkeit von Verbindungen mit selbstbohrenden Holzschrauben mit Vollgewinde vol. 4. Karlsruhe: KIT Scientific Publishing, Karlsruher Berichte zum Ingenieurholzbau; 2006.
[3] Hansen K. Mechanical properties of self-tapping screws and nails in wood. Can J Civ Eng 2002;29:725–33.
[4] RinghoferA., Brandner R, Schickhofer G. A universal approach for withdrawal properties of self-tapping screws in solid timber and laminated timber products. In: Proceedings of the 2nd International Network on Timber Engineering Research (INTER 2015), Sibenik (Croatia), paper INTER/48-7-1 (USB drive); 2015.
[5] EN 1995-1-1. Design of timber structures – Part 1–1: general – common rules and rules for buildings. Brussels, Belgium: European Committee for Standardization (CEN); 1995.
[6] Tomasi R, Crosatti A, Piazza M. Theoretical and experimental analysis of timber-to-timber joints connected with inclined screws. Constr Build Mater 2010;24:1560–71.
[7] Girhammar UA, Jacquier N, Källsner B. Stiffness model for inclined screws in shear-tension mode in timber-to-timber joints. Eng Struct 2017;136:580–95.
[8] Giongo I, Piazza M, Tomasi R. Out of plane refurbishment techniques of existing timber floors by means of timber to timber composite structures. In: Proceedings of WCTE 2012 – World Conference on Timber Engineering, Auckland, Canada, July 16-19 (CD Rom); 2012.
[9] Giongo I, Piazza M, Tomasi R. Cambering of timber composite beams by means of screw fasteners. J Heritage Conserv 2012;32:133–6.
[10] Opazo A, Bustos C. Study of the lateral strength of timber joints with inclined self-tapping screws. In: Proceedings of the 51st International Convention of Society of Wood Science and Technology, Concepcion (Chile), paper WS-39 (USB drive); 2008.
[11] Ringhofer A, Schickhofer G. Investigations concerning the force distribution along axially loaded Self-Tapping Screws. Aicher S, Reinhardt HW, Garrecht H, editors. Materials and joints in timber structures. RILEM Bookseries (vol. 9), Springer, Dordrecht; 2015.
[12] Hossain A, Popovski M, Tannert T. Cross-laminated timber connections assembled with a combination of screws in withdrawal and screws in shear. Eng Struct 2018;168:1–11.
[13] Berardinucci B, Di Nino S, Gregori A, Fragiacomo M. Mechanical behavior of timber–concrete connections with inclined screws. Int J Comput Methods Exp Measure, Special Issue Timber Structures 2017;5(6):807–20.
[14] Symons D, Persaud R, Stanislaus H. Slip modulus of inclined screws in timber-concrete floors. Struct Build 2010;163(SB4):245–55.
[15] Jacquier N, Girhammar UA. Evaluation of bending tests on composite glulam-CLT beams connected with double-sided punched metal plates and inclined screws. Constr Build Mater 2015;95:762–73.
[16] Schiro G, Giongo I, Sebastian W, Riccadonna D, Piazza M. Testing of timber-to-timber screw-connections in hybrid configurations. Constr Build Mater 2018;171:170–86.
[17] Silva C, Branco JM, Ringhofer A, Lourenco PB, Schickhofer G. The influence of moisture content variation, number and width of gaps on the withdrawal resistance of self tapping screws inserted in cross laminated timber. Constr Build Mater 2016;125:1205–15.
[18] Descamps T, Lalisse D, Datoussaid S. 3D FEM modeling of slender laterally loaded timber fasteners. In: Proceedings of the 12th International Conference on Fracture, Ottawa, Canada, July 12–17; 2009.
[19] Xu BH, Bouchaïr A, Taazount M, Vega EJ. Numerical and experimental analyses of multiple-dowel steel-to-timber joints in tension perpendicular to grain. Eng Struct 2009;31:2357–67.
[20] Xu BH, Taazount M, Bouchaïr A, Racher P. Numerical 3D finite element modelling and experimental tests for dowel-type timber joints. Constr Build Mater 2009;23:3043–52.
[21] Kharouf N, McClure G, Smith I. Elasto-plastic modeling of wood bolted connections. Comput Struct 2003;81:747–54.
[22] dos Santos CL, Morais JJL, de Jesus AMP. Mechanical behaviour of wood T-joints – experimental and numerical investigation. Frattura ed Integrità Strutturale 2015;31:23–37. https://doi.org/10.3221/IGF-ESIS.31.03.
[23] Chen CJ, Lee TL, Jeng DS. Finite element modeling for the mechanical behavior of dowel-type timber joints. Comput Struct 2003;81:2731–8.
[24] Dias AMPG, Van de Kuilen JW, Lopes S, Cruz H. A non-linear 3D FEM model to simulate timber–concrete joints. Adv Eng Softw 2007;38:522–30.
[25] Khelifa M, Khennane A, El Ganaoui M, Celzard A. Numerical modelling of 3D dowelled timber joints using advanced fully coupled hydro-mechanical constitutive equations. Mech Ind 2015;16(501). https://doi.org/10.1051/meca/2015034.
[26] van de Kuilen JWG, Dejong M. 3D-numerical modelling of DVW-reinforced timber joints. In: Proceedings of WCTE 2004 – World Conference on Timber Engineering, Espoo Finland (CD Rom); 2004.
[27] Hassanieh A, Valipour HR, Bradford MA, Sandhaas C. Modelling of steel-timber composite connections: validation of finite element model and parametric study. Eng Struct 2017;138:35–49.
[28] Karagiannis V, Malaga-Chuquitaype C, Elghazouli AY. Modified foundation modelling of dowel embedments in glulam connections. Constr Build Mater 2016;102:1168–79.
[29] ABAQUS computer software, v.6.14, Simulia, Dassault Systemes.
[30] ABAQUS documentation and uses' guide, v.6.14, Simulia, Dassault Systemes.
[31] Avez C, Descamps T, Serrano E, Léoskool L. Finite Element modelling of inclined screwed timber to timber connections with a large gap between the elements. Eur J Wood Wood Prod 2016;74:467–71.
[32] Zhang ZJ, Paulino GH, Celes W. Extrinsic cohesive modelling of dynamic fracture and microbranching instability in brittle materials. Int J Numer Meth Eng 2007;72:893–923.
[33] Katnam KB, Crocombe AD, Khoramishad H, Ashcroft IA. The static failure of adhesively bonded metal laminate structures: a cohesive zone approach. J Adhes Technol 2011;25:1131–57.
[34] Dogan F, Hadavinia H, Donchev T, Bhonge PS. Delamination of impacted composite structures by cohesive zone interface elements and tiebreak contact. Central Eur J Eng 2012;2(4):612–26.
[35] Xu W, Wei Y. Influence of adhesive thickness on local interface fracture and overall strength of metallic adhesive bonding structures. Int J Adhes Adhes 2013;40:158–67.
[36] Gao W, Xiang J, Chen S, Yin S, Zang M, Zheng X. Intrinsic cohesive modeling of impact fracture behavior of laminated glass. Mater Des 2017;127:321–5.
[37] Bedon C, Machalicka K, Eliasova M, Vokac M. Numerical modelling of adhesive connections including cohesive damage. In: Proceedings of challenging glass 6 – conference on architectural and structural applications of glass, TU Delft (The Netherlands), USB drive; 2018.
[38] Aira JR, Descamps T, Van Parys L, Léoskool L. Study of stress distribution and stress concentration factor in notched wood pieces with cohesive surfaces. Eur J Wood Wooden Products 2015;73:325–34.
[39] Ardalany M, Fragiacomo M, Moss P. Modeling of laminated veneer lumber beams with holes using cohesive elements. J Struct Eng 2016;142(1). https://doi.org/10.1061/(ASCE)ST.1943-541X.0001338.
[40] Saavedra Flores EI, Saavedra K, Hinojosa J, Chandra Y, Das R. Multi-scale modelling of rolling shear failure in cross-laminated timber structures by homogeneisation and cohesive zone models. Int J Solids Struct 2016;81:219–32.
[41] Bedon C, Fragiacomo M. Three-dimensional modelling of notched connections for timber-concrete composite beams. Struct Eng Int 2017;27(2):184–96. https://doi.org/10.2749/101686617X14881932435295.
[42] Janssen SB. Numerical modelling of dowelled connections in Laminated Veneer Lumber [Master Thesis] The Netherlands: Delft University of Technology; 2017 available online (uuid: 89a15968-c659-4939-ac9b-1b487c9a976b).
[43] Bedon C, Fragiacomo M, Tamagnone G. Numerical investigation on timber-to-timber joints and composite beams with inclined self-tapping screws. In: Proceedings of WCTE 2018 – World Conference on Timber Engineering, August 20–23, Seoul, Republic of Korea (CD Rom); 2018.
[44] EN 12512:2001. Timber structures – Test Methods – Cyclic testing of joints made with mechanical fasteners. European Committee for Standardization (CEN), Brussels, Belgium.
[45] EN 26891. Joints made with mechanical fasteners – general principles for the determination of strength and deformation characteristics. Brussels, Belgium: European Committee for Standardization (CEN); 1991.
[46] EN 1194. Timber structures – glued laminated timber – strength classes and determination of characteristic values. Brussels, Belgium: European Committee for Standardization (CEN); 1999.
[47] ETA-11/0190. Würth self-tapping screws – Self-tapping screws for use in timber constructions. European Organisation for Technical Approvals (EOTA).
[48] Rothoblaas – WT Double thread connector – Technical Data Sheet (available online, accessed May 2018, https://www.rothoblaas.com/products/fastening/screws).
[49] Newmark NM, Siess CP, Viest IM. Tests and analysis of composite beams with incomplete interaction. Proc Soc Exptl Stress Anal 1951;9(1):75–92.
[50] Mohler K. Uber das Tragverhalten von Biegetragern und Druckstaben mit zusammengesetztem Querschnitt und nachgiebigen Verbindungsmitteln. Habilitation: TH Karlsruhe; 1956.
[51] Lukaszewska E. Development of prefabricated timber-concrete composite floors [Doctoral Thesis] Lulea University of Technology; 2009 ISSN 1402-1544, ISBN 978-91-86233-85-3. Available online (https://www.diva-portal.org/smash/get/diva2:991048/FULLTEXT01.pdf).
[52] Kenel AA. Zur Berechnung von Holz-Beton-Verbundkonstruktionen. Forschungsbericht 115/42. Abteilung Holz: EMPA; 2000.
[53] Frangi AA. Brandverhalten von Holz-Beton-Verbunddecken. IBK Bericht Nr. 269, Birkhauser Verlag Basel: Institut fur Baustatik und Konstruktion (IBK), ETH Zurich; 2001.
[54] Cosenza E, Mazzolani S. Linear-elastic analysis of composite beams with partial shear interaction. Proceedings of the First Italian workshop on composite structures. Italy: University of Trento; 1993.
[55] Girhammar UA, Pan DH. Exact analysis of partially composite beams and beam-columns. Int J Mech Sci 2007;49(2):239–55.
[56] Martinelli E, Faella C, Di Palma G. Shear-flexible steel-concrete composite beams in partial interaction: closed-form "exact" expression of the stiffness matrix. J Eng Mech 2012;138:151–63.
[57] Amadio C, Bedon C. Buckling of laminated glass elements in compression. J Struct Eng 2011;137(8):803–10.
[58] Neagoe CA, Gil L. Analytical procedure for the design of PFRP-RC hybrid beams including shear interaction effects. Compos Struct 2015;132:122–35.
[59] Oudjene M, Meghalt E-M, Ait-Aider H, Batoz J-L. Non-linear finite element modelling of the structural behaviour of screwed timber-to-concrete composite connections. Compos Struct 2013;102:20–8.
[60] Dias AMPG, Jorge LFC. The effect of ductile connectors on the behaviour of timber-

concrete composite beams. Eng Struct 2011;33:3033–42.
[61] Meghalt E-M, Oudjene M, Ait-Aider H, Batoz J-L. A new approach to model nailed and screwed timber joints using the finite element method. Constr Build Mater 2013;41:263–9.
[62] Auclari SC, Sorelli L, Salenikovich A. Simplified nonlinear model for timber-concrete composite beams. Int J Mech Sci 2016;117:30–42.
[63] Izzi M, Polastri A, Fragiacomo M. Modelling the mechanical behaviour of typical wall-to-floor connection systems for cross-laminated timber structures. Eng Struct 2018;162:270–82.
[64] Laggner TM, Flatscher G, Schickhofer G. Combined loading of self-tapping screws. In: Proceedings of WCTE 2016 – World Conference on Timber Engineering, August 22-25, Vienna, Austria (CD Rom); 2016.
[65] Jockwer R, Steiger R, Frangi A. Fully threaded self-tapping screws subjected to combined axial and lateral loading with different load to grain angles. In: Aicher, Reinhardt, Garrecht, editors. Materials and Joints in Timber Structures, RILEM Bookseries, vol. 9. Springer, Dordrecht; 2014 pp. 265–272.
[66] Leoskool L, Serrano E, Descamps R. COST Action FP1004: Short Term Scientific Mission at Lund University – Finite element modelling of a new structural insulated panel based on CLT using Abaqus. Technical Report; 2014.
[67] Leoskool L, Descamps T. Development of a structural insulated panel (SIP) with wood-based material. In: Proceedings of COST Action FP1004 Conference – Experimental Research in Timber, pp. 36–41, Prague, Czech Republic; 2014.
[68] Naderer E, Franke S, Franke B. Numerical simulation of reinforced timber structures perpendicular to the grain. In: Proceedings of WCTE 2016 – World Conference on Timber Engineering, August 22-25, Vienna, Austria (CD Rom); 2016.
[69] Murase Y. Friction of wood sliding on various materials. J Faculty Agric, Kyushu University 1984;28(4):147–60.
[70] Fortino S, Hradil P, Salminen LI, De Magistris F. A 3D micromechanical study of deformation curves and cell wall stresses in wood under transverse loading. J Mater Sci 2015;50(1):482–92.
[71] EN 338. Structural timber – strength classes. Brussels, Belgium: European Committee for Standardization (CEN); 2003.